Journal of Pathology
J Pathol October 2023; **261**: 169–183
Published online 9 August 2023 in Wiley Online Library
(wileyonlinelibrary.com) DOI: 10.1002/path.6161

ORIGINAL ARTICLE

Intravascular hemolysis triggers NAFLD characterized by a deregulation of lipid metabolism and lipophagy blockade

Sandra Rayego-Mateos[1,2], José Luis Morgado-Pascual[2,3], Cristina García-Caballero[2], Iolanda Lazaro[4], Aleix Sala-Vila[4], Lucas Opazo-Rios[5], Sebastian Mas-Fontao[6,7,8], Jesús Egido[6,8], Marta Ruiz-Ortega[1] and Juan Antonio Moreno[2,3,7]*

[1] *Molecular and Cellular Biology in Renal and Vascular Pathology. IIS-Fundación Jiménez Díaz, Universidad Autónoma Madrid, Madrid, Spain*
[2] *Maimonides Biomedical Research Institute of Cordoba (IMIBIC), Hospital Universitario Reina Sofía, Cordoba, Spain*
[3] *Department of Cell Biology, Physiology and Immunology, University of Cordoba, Cordoba, Spain*
[4] *Cardiovascular Risk and Nutrition, Hospital del Mar Medical Research Institute (IMIM), Barcelona, Spain*
[5] *Health Science Faculty, Universidad de Las Américas, Concepción-Talcahuano, Chile*
[6] *Spanish Biomedical Research Centre in Diabetes and Associated Metabolic Disorders (CIBERDEM), Madrid, Spain*
[7] *Biomedical Research Networking Center on Cardiovascular Diseases (CIBERCV), Madrid, Spain*
[8] *Instituto de Investigación Sanitaria (IIS)-Fundación Jiménez Díaz, Universidad Autónoma, Madrid, Spain*

*Correspondence to: JA Moreno, Department of Cell Biology, Physiology and Immunology, University of Cordoba, 14014 Cordoba, Spain.
E-mail: juan.moreno@uco.es

Abstract

Intravascular hemolysis is a common feature of different clinical entities, including sickle cell disease and malaria. Chronic hemolytic disorders are associated with hepatic damage; however, it is unknown whether heme disturbs lipid metabolism and promotes liver steatosis, thereby favoring the progression to nonalcoholic fatty liver disease (NAFLD). Using an experimental model of acute intravascular hemolysis, we report here the presence of liver injury in association with microvesicular lipid droplet deposition. Hemolysis promoted serum hyperlipidemia and altered intrahepatic triglyceride fatty acid composition, with increments in oleic, palmitoleic, and palmitic acids. These findings were related to augmented expression of transporters involved in fatty acid uptake (CD36 and MSR1) and deregulation of LDL transport, as demonstrated by decreased levels of LDL receptor and increased PCSK9 expression. Hemolysis also upregulated hepatic enzymes associated with cholesterol biosynthesis (SREBP2, HMGC1, LCAT, SOAT1) and transcription factors regulating lipid metabolism (SREBP1). Increased LC3II/LC3I ratio and p62/SQSTM1 protein levels were reported in mice with intravascular hemolysis and hepatocytes stimulated with heme, indicating a blockade of lipophagy. In cultured hepatocytes, cell pretreatment with the autophagy inductor rapamycin diminished heme-mediated toxicity and accumulation of lipid droplets. In conclusion, intravascular hemolysis enhances liver damage by exacerbating lipid accumulation and blocking the lipophagy pathway, thereby promoting NAFLD. These new findings have a high translational potential as a novel NAFLD-promoting mechanism in individuals suffering from severe hemolysis episodes.

Keywords: intravascular hemolysis; heme; liver damage; NAFLD; lipophagy; lipid metabolism; lipid accumulation

Received 5 November 2022; Revised 30 May 2023; Accepted 14 June 2023

No conflicts of interest were declared.

Introduction

Intravascular hemolysis is a common feature of various clinical entities, such as sickle cell disease (SCD), malaria, and thrombotic microangiopathies, among others [1–3]. Hemolysis promotes massive release of erythrocyte-breakdown products into the bloodstream, such as hemoglobin (Hb) and heme. These cytotoxic molecules can accumulate in various tissues, including the liver [3–7]. Thus, hepatic injury has been described in 10–40% of patients with SCD and in animal models of hemolytic pathologies [8–12].

Nonalcoholic fatty liver disease (NAFLD) is an emerging disease with elevated prevalence (20–30% of the general population) [13]. NAFLD depicts different manifestations of hepatic damage, ranging from steatosis to steatohepatitis (hepatocyte ballooning, inflammatory clusters, with or without fibrosis) and potentially progression to hepatocellular carcinoma [14,15]. NAFLD is a consequence of triglyceride (TG) accumulation elicited by the augmentation of fatty acids uptake and *de novo* lipogenesis (DNL) and altered lipid efflux [16]. This exacerbated accumulation of lipids surpasses fatty acid oxidation and its exportation,

thereby favoring intrahepatic lipid deposition [17] and dyslipidemia [18–22]. However, the effect of hemolysis on lipid metabolism has not been fully analyzed, and the few studies performed to date are controversial, with some reporting hyperlipidemia, whereas other showed no changes or decreased levels of circulating lipids [23–25]. Hence, it is very important to fully study the role of hemolysis on hepatic lipid metabolism and the pathological consequences.

Autophagy maintains cellular homeostasis by eliminating misfolded proteins, aggregates, or spoiled organelles in lysosomal vesicles [26]. Autophagy plays a critical role in the development of steatosis and steatohepatitis [27–29]. Several studies described the term lipophagy as the autophagy process that degrades lipid droplets through lysosomes in the liver [30]. Lipophagy may be deregulated in hepatic damage [31,32]. However, no previous study had analyzed the role of heme accumulation in liver lipophagy and whether heme-mediated lipophagy induced fatty acid accumulation and subsequent alteration of lipid metabolism. To answer these questions, we developed an experimental model of intravascular hemolysis in mice and cultured hepatic cells, where we explored the effect of heme accumulation on liver injury as well as the potential mechanisms implicated in this pathogenic effect.

Materials and methods

Cultured cells

Human liver hepatocellular carcinoma cells (HepG2 cell line; ATCC® HB-8065; ATCC; Manassas; VA, USA) were stimulated with 5 μM of recombinant human Heme (Catalog No. H9039, Sigma-Aldrich, St. Louis, MO, USA) in the presence/absence of rapamycin (1 μM; Sigma-Aldrich). Heme concentrations were based on previously published dose–response experiments [33]. Cell viability was analyzed using the MTT assay (Thiazolyl Blue tetrazolium bromide, Sigma-Aldrich). An extended description is provided in Supplementary materials and methods.

Experimental animal models

The study was conducted according to Directive 2010/63/EU of the European Parliament and was approved by the Institutional Animal Care and Use Committee (IIS-Fundación Jimenez Diaz). The following experimental models were performed in 9-week-old male C57BL/6 mice.

Intravascular hemolysis

Phenylhydrazine (PHE) (150 mg/kg of body weight, Catalog No. 114715, Sigma-Aldrich) was injected (i.p.) in mice [33]. Mice (n = 5–6/group) were euthanized 72 h after PHE injection.

Hemin overload

Hemin (200 μl; 70 μmol/kg, Catalog No. H9039; Sigma-Aldrich) was injected (i.p.) in mice (n = 5–8/group), and the animals were euthanized 72 h later.

High carbonyl iron diet model

Mice (n = 5–10/group) were fed for 8 weeks with a control diet (C1000 diet; Altromin, Lage, Germany) or high carbonyl iron diet (C1000 control diet plus carbonyl iron 20 g/kg; Altromin) and then sacrificed.

At the time of sacrifice, animals were anesthetized with 5 mg/kg xylazine (Rompun, Bayer AG, Germany) and 35 mg/kg ketamine (Ketolar, Pfizer, New York, USA) and liver perfused *in situ* with cold saline before removal. Then liver portions were fixed in buffered formalin for immunohistochemistry studies or immediately frozen in liquid nitrogen for gene expression and protein studies. An extended description is provided in Supplementary materials and methods.

Biochemical parameters

Serum lipid profiles and liver biochemical parameters were assessed at the central laboratories of our Institution. Total heme concentration in liver was determined with a commercial kit (Catalog No. MAK316; Sigma-Aldrich). Fatty acid methyl esters (FAMEs) from liver TGs were determined as described previously [16]. Total fatty acids were estimated as the sum of all the fatty acid species in liver TGs.

Oil Red O staining

Determination of lipid droplets in liver tissues and in cultured cells was performed with Oil Red O staining. More detail is provided in Supplementary materials and methods.

Histology and immunohistochemistry

Paraffin-embedded liver sections (3 μm) were stained with hematoxylin and eosin (Catalog Nos. 10034813 and 6766007, Thermo Fisher Scientific, Waltham, MA, USA) and signs of histological injury assessed. LDL receptor (LDLR) immunohistochemistry is described in Supplementary materials and methods.

Western blotting

Proteins from tissues or cultured cells were isolated in lysis buffer and analyzed by western blotting. Primary antibodies were detected with an appropriate horseradish peroxidase (HRP)-conjugated secondary antibody and then developed using an ECL chemiluminescence kit (Amersham, Little Chalfont, UK). Blots were scanned using a Gel Doc™ EZ imager (Thermo Fisher Scientific) and analyzed with the Image Lab 3.0 software (BioRad Laboratories, Hercules, CA, USA).

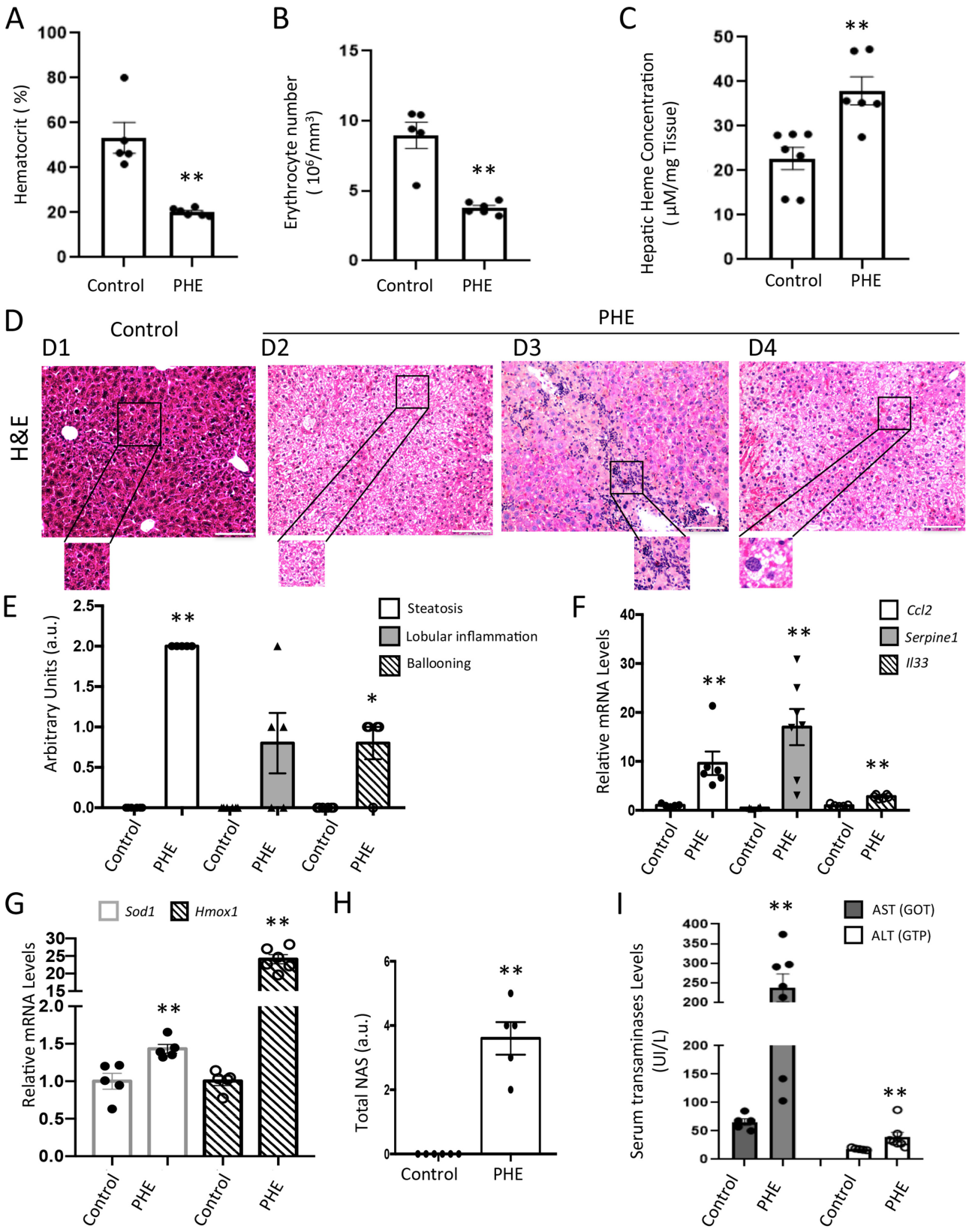

Figure 1. Experimental intravascular hemolysis induces hepatic damage. Mice were injected with PHE (150 mg/kg) or saline (control) and then were sacrificed at 72 h. (A) Hematocrit and (B) erythrocyte number assessments. (C) Heme content in liver tissue. (D) Representative images showing histopathological changes in liver tissue by H&E staining in control (D1) and PHE-injected mice (D2-4; D2: steatosis foci; D3: Inflammatory infiltrate foci, D4: ballooning). Bar score (100 µm). (E) Semiquantitative determination of steatosis, lobular inflammation, and hepatocyte ballooning in livers of PHE-injected mice. (F) Hepatic gene expression of *Il-33; Ccl2* and *Serpine* mRNA levels as determined by RT-qPCR. (G) Hepatic gene expression of antioxidant markers superoxide dismutase (*Sod1*) and heme oxygenase 1 (*Hmox1*), as determined using RT-qPCR. (H) NAFLD activity score (NAS) assessment. (I) Serum levels of transaminases (AST and ALT). Mean ± SEM of five to eight mice per group. $^{*}p < 0.05$; $^{**}p < 0.01$ versus control.

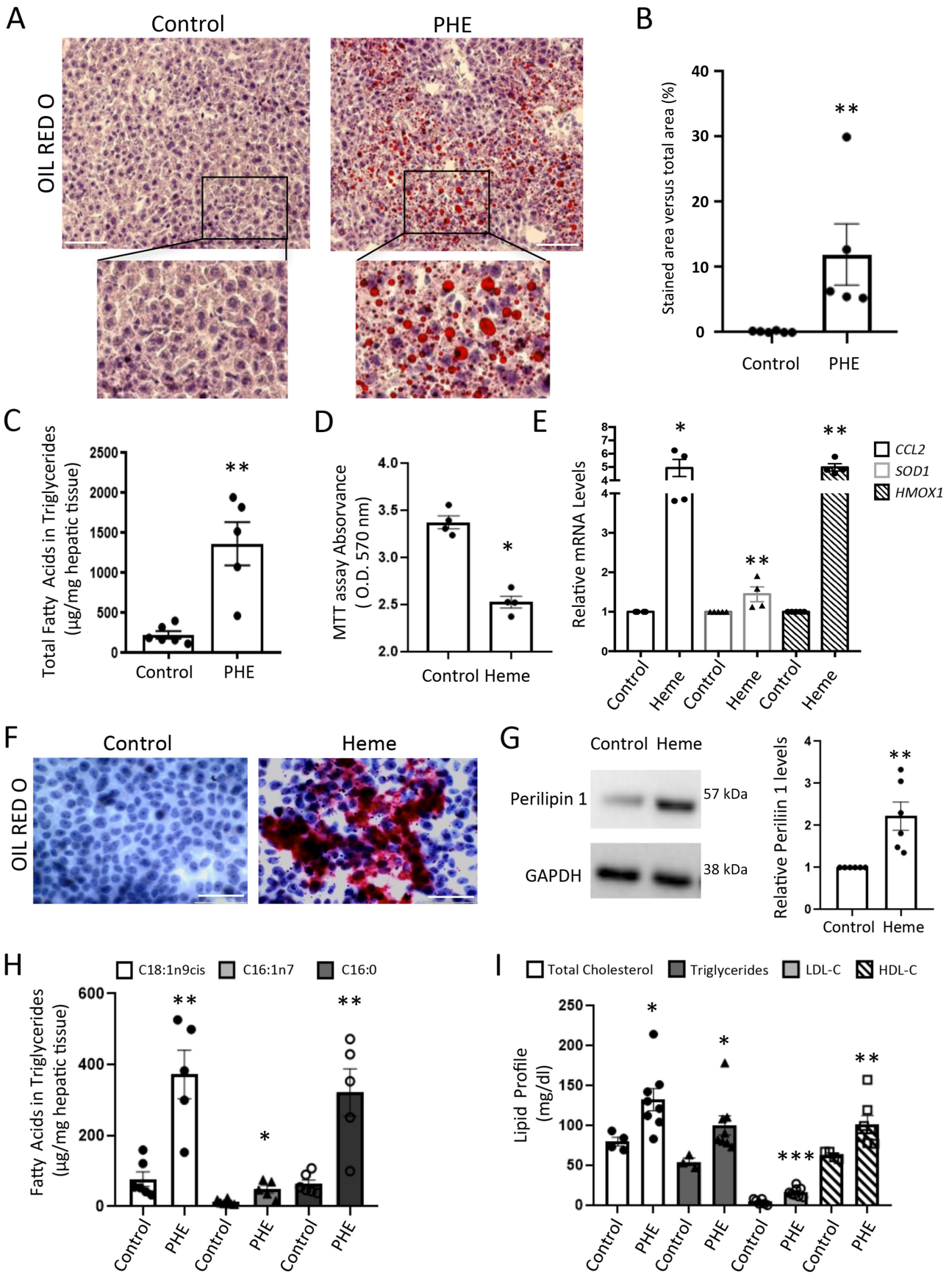

Figure 2 Legend on next page.

Gene expression studies

Total RNA was isolated from cultured cells and tissues using Trizol (Invitrogen, Waltham, MA, USA). cDNA was synthesized using a High-Capacity cDNA Archive Kit (Applied Biosystems, Waltham, MA, USA). Multiplex real-time PCR was performed on an ABI Prism 7500 PCR system (Applied Biosystems) using Applied Biosystems expression assays or IDT PrimeTime™ predesigned qPCR assays. More detail is provided in Supplementary materials and methods.

Analysis of ^{13}C-acetate in fatty acids

Control and PHE-injected mice received ^{13}C sodium acetate (0.3 M, in drinking water; Sigma-Aldrich) 4 h prior to PHE injection. Animals were sacrificed 72 h after PHE injection. Liver fatty acids were extracted and methylated as described previously [34] and quantified using gas chromatography–mass spectrometry (GC–MS).

Statistical analysis

Statistical significance was assessed using GraphPad Prism 5.0 (GraphPad Software, San Diego, CA, USA). Comparisons between groups were performed using a parametric unpaired two-sided *t*-test if the data followed a normal distribution (confirmed by a Shapiro–Wilk normality test) and the homogeneity of variances (tested with F-test). The data are presented as mean ± SEM. Lipid discriminant and clustering analysis was carried out respectively using an orthogonal partial least squares discriminant analysis (oPLS-DA) and Euclidean hierarchical clustering with the MetaboAnalyst R 2.0 package (https://www.metaboanalyst.ca/; accessed October 6, 2023). Differences were considered statistically significant when the p value was <0.05.

See Supplementary materials and methods for fuller details and descriptions of Oil Red O staining, protein studies, histology and immunohistochemistry, MTT viability studies, lipidic profile determination, lipid extraction from liver tissue, and analysis of ^{13}C label acetate in fatty acids.

Results

Intravascular hemolysis causes lipid accumulation, inflammation, and liver damage

To study the effect of heme accumulation on liver injury, we developed an experimental model of massive intravascular hemolysis. Mice were injected with PHE to promote the lysis of erythrocytes and the subsequent release of high quantities of heme into the bloodstream [33]. As expected, administration of PHE reduced hematocrit and erythrocyte number (Figure 1A,B) and increased liver iron content (Figure 1C). In the livers of mice with hemolysis, we detected inflammatory clusters/foci (Figure 1D, panel D3, and Figure 1E), as well as increased gene expression of inflammatory mediators such as *CC chemokine ligand 2* (*Ccl2*), *Serpine*, and *Interleukin 33 (Il33)* (Figure 1F). In addition, increased expression of antioxidant markers, such as superoxide dismutase 1 (*Sod1)* and heme oxygenase 1 (*Hmox1*), was observed in hepatic tissue of mice with hemolysis (Figure 1G).

Histological analysis of mice with hemolysis revealed significant alterations in hepatic tissue, characterized by foci of microvesicular steatosis and hepatocellular ballooning (Figure 1D, panels D2 and D4, and Figure 1E). An increment in total NAFLD activity score (NAS) was also observed in the hepatic tissue of mice with hemolysis (Figure 1H). In line with the morphological data, we noted increased serum levels of the liver injury markers aspartate aminotransferase (ASAT) and alanine aminotransferase (ALAT) after induction of hemolysis (Figure 1I). Oil Red O staining confirmed the presence of microvesicular lipid deposits (Figure 2A,B) and an increase of total fatty acids in the liver of PHE-injected mice (Figure 2C). To further demonstrate whether heme could directly regulate lipid deposition in the liver, we performed two additional experimental models (hemin overload and high carbonyl iron diet). In both experimental models we observed histological hepatic damage characterized by ballooning, inflammatory infiltrates, and microvesicular lipid deposition (supplementary material, Figures S1A,B and S2A,B). Steatosis was generalized after high carbonyl iron diet consumption, whereas hemin administration only induced small foci steatosis (supplementary material, Figures S1A,B and S2A,B). In both models, an increment in total NAS liver

Figure 2. Intravascular hemolysis induces hepatic lipidic deposition in mice and cultured HepG2 cells. (A) Lipid deposition was evaluated using Oil Red O staining of OCT-embedded liver sections of PHE- (150 mg/kg) or saline (vehicle)-injected mice. Figures are representative of each experimental group. Scale bar, 100 μm. (B) Quantification of Oil Red O stained area versus total area. (C) Total fatty acid content in TG. Mean ± SEM of five to eight mice per group. *$p < 0.05$; **$p < 0.01$; ***$p < 0.001$ versus control. (D) Cell viability assay of heme-stimulated HepG2 cells. (E) mRNA levels for inflammatory (*CCL2*) and antioxidant markers (*SOD1*; *HMOX-1*) were assessed using RT-qPCR in HepG2 cells treated with heme (5 μM) for 6 h. Mean ± SEM of three to six experiments, *$p < 0.05$; **$p < 0.01$ versus control. (F) HepG2 cells were stimulated with heme (5 μM) for 24 h before assessing lipid deposition using Oil Red O. Scale bar, 100 μm. (G) Protein levels of Perilipin 1 assessed by western blotting. GAPDH levels were used as loading controls. Figure shows a representative western blot and the quantification of the data. (H) Fatty acid composition of TGs by GC–MS in liver tissue samples: oleic acid (C18:1n9 cis), palmitoleic acid (C16:1n7), and palmitic acid (C16:0) in TG. (I) Lipid profile in serum samples: total cholesterol, TGs, LDL-c, and HDL-c. Mean ± SEM of five to eight mice per group. *$p < 0.05$; **$p < 0.01$; ***$p < 0.001$ versus control.

score was observed after hemin injection and high carbonyl iron fed mice compared to its respective controls (supplementary material, Figures S1C and S2C).

Finally, we conducted *in vitro* studies in human hepatocytes (HepG2 cells) stimulated with heme for 24 h. In these conditions, we found a reduction of hepatocyte viability (Figure 2D) and an augmented expression of inflammatory mediators and components of the antioxidant response (Figure 2E). Importantly, heme-treated cells showed a significant increase in microvesicular lipid content (Figure 2F) and increased expression of Perilipin 1, encoding a lipid droplet-associated protein (Figure 2G). Taken together, these data indicate that heme causes lipid accumulation in hepatocytes.

Intravascular hemolysis modifies hepatic fatty acid homeostasis

Having demonstrated the direct effect of iron overload on lipid accumulation, we next analyzed the composition of fatty acids of the intrahepatic TG subfractions. Compared to control, mice with hemolysis had a significant increase in oleic acid (C18:1n9 cis) and palmitoleic acid (C16:1n7) (Figure 2H), major fatty acid species in hepatic TGs [35]. There was also an increase of the lipotoxic palmitic acid (C16:0) levels in TGs isolated from livers of PHE-injected mice (Figure 2H). More specific analysis based on the differences in fatty acid composition in the hepatic TG subfractions allowed us to discriminate each experimental group using oPLS-DA (supplementary material, Figure S3A). Furthermore, hierarchical clustering showed differential lipidic profiles that were associated with lipidic composition in response to hemolysis (supplementary material, Figure S3B). Intravascular hemolysis in mice also raised the serum concentration of total cholesterol, LDL-c, HDL-c, and TGs (Figure 2I).

Intravascular hemolysis modulates fatty acid uptake both *in vivo* and *in vitro*

We next examined possible mechanisms responsible for the increased hepatic accumulation of lipids in response to hemolysis. In the livers of PHE-injected mice, we detected a significant increase in gene and protein expression levels of CD36 and MSR1, two key proteins involved in the hepatic uptake of fatty acids [36] (Figure 3A–C). Since hemolysis was associated with serum hypercholesterolemia, the expression of proprotein convertase subtilisin/kexin type 9 (PCSK9) and LDLR was evaluated [37]. Our results revealed that intravascular hemolysis increased PCSK9 mRNA and protein expression in the liver (Figure 3D,F), whereas reduced hepatic protein LDLR levels were observed (Figure 3E,F). Similar effects were found in heme-stimulated HepG2 cells (Figure 3G–I). Taken together, these data suggest a direct effect of heme on lipid uptake in the liver.

Intravascular hemolysis elicits hepatic deregulation of fatty acid biosynthesis in mice

We first analyzed three transcription factors that regulate lipid metabolism, named sterol regulatory element binding protein 1 (*Srebp1*), carbohydrate response element-binding protein (*ChREBP/mLxip1*), and peroxisome proliferator-activated receptor-γ (*Pparγ*). Mice subjected to intravascular hemolysis showed a significant reduction in gene expression levels of *Chrebp/mLxip1* and *Pparγ* (Figure 4A), while *Srebp1* was increased (Figure 4A). These results were confirmed at the protein level as high expression of the precursor, and mature forms of SREBP1 was noted (Figure 4B). Experiments in heme-stimulated HepG2 cells also reported increased gene and protein expression of SREBP1 (Figure 4C,D).

Considering that both oleic and palmitoleic acids are end products of DNL (*via* acetyl-coA produced by either lipids or glucose), we further investigated whether the hepatic increase of these species was related to DNL. In this regard, hemolysis reduced the gene expression and protein levels of fatty acid synthetase (*Fasn*), which is involved in DNL, in particular C16:0 [17] (Figure 4A,E). To further rule out the role of DNL, mice received ^{13}C-acetate in drinking water from 4 h before PHE administration until sacrifice (72 h after induction of hemolysis). As reported by GC–MS analysis, mice receiving ^{13}C-acetate showed higher incorporation of this tracer, independently of the presence of hemolysis. However, in the group of hemolyzed mice, ^{13}C-acetate enrichment in palmitic acid (C16:0), stearic acid (C 18:0), and oleic acid (C18:1) species was lower compared to controls (supplementary material, Figure S4A–C).

In contrast, in livers from mice with hemolysis, no significant differences in protein levels were observed in diglyceride acyltransferase 2 (*Dgat2*), an enzyme that participates in the synthesis of TGs *in vivo* (Figure 4E). However, the protein levels of this enzyme were increased in cultured hepatocytes stimulated with heme (Figure 4F).

Intravascular hemolysis in mice causes hepatic deregulation of cholesterol biosynthesis

Hemolysis increased hepatic mRNA levels for enzymes involved in cholesterol biosynthesis [hydroxy-3-methylglutaryl-coenzyme A synthase 1 (*Hmgc1*)] and the formation of cholesterol esters [lecithin-cholesterol acyltransferase (*Lcat*)] and Sterol O-Acyltransferase 1 (*Soat1*) (Figure 4G). In addition, PHE-injected mice also showed increased gene and protein levels of *srebp2*, the transcription factor that regulates cholesterol biosynthesis (Figure 4G,H). Experiments in heme-stimulated HepG2 cells also manifested increased SREBP2 gene and protein expression (Figure 4C,I). The increase in these markers suggests an upregulation of cholesterol biosynthesis. To confirm this hypothesis, we determined the incorporation of ^{13}C-acetate into the cholesterol fraction in the liver of mice with hemolysis by GC–MS. As shown in supplementary material, Figure S4D, the livers of mice with

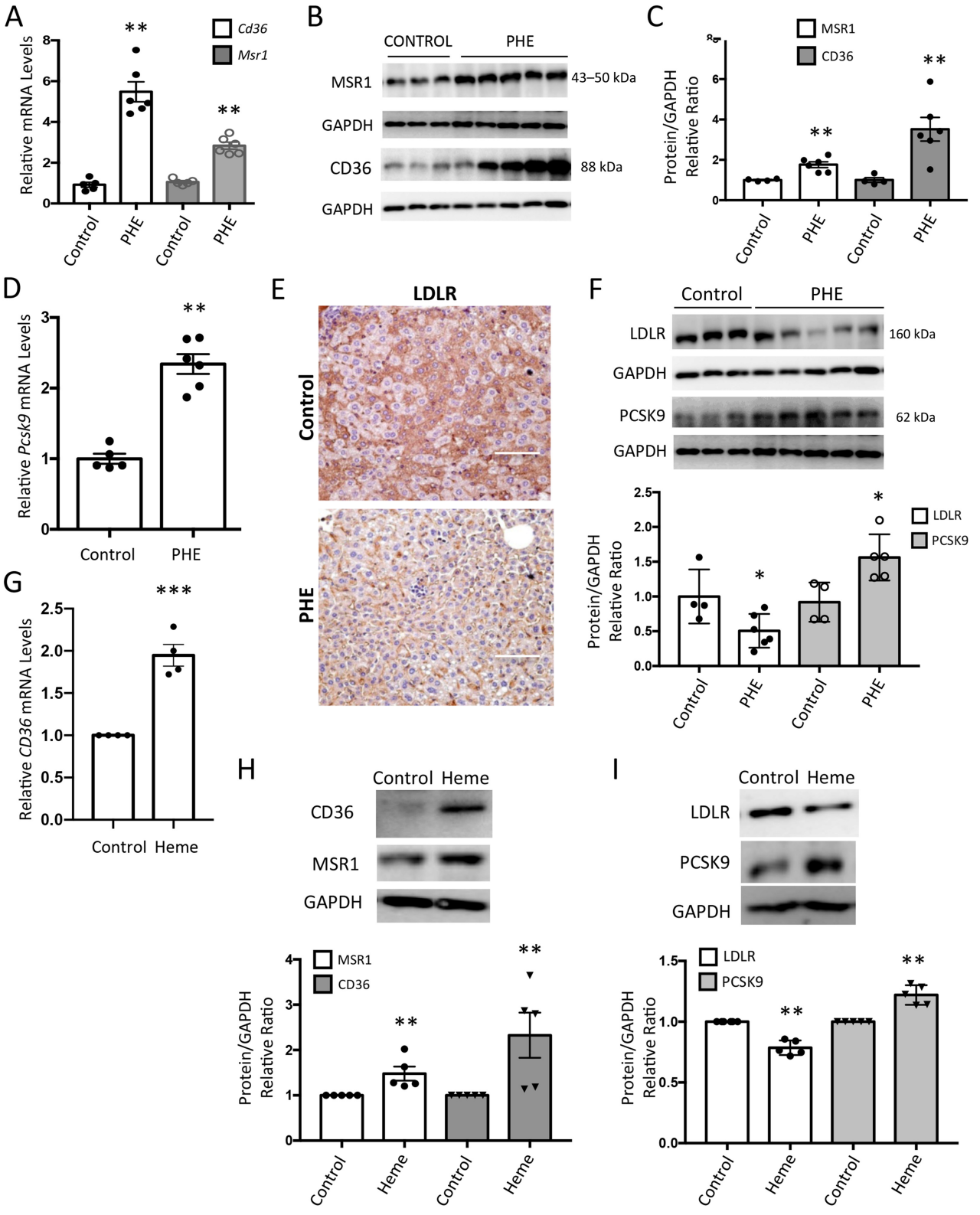

Figure 3. Intravascular hemolysis increases lipid uptake mechanisms, including LDLR/PCSK9 modulation in mice liver and HepG2 cells. Mice were injected with PHE (150 mg/kg) or saline (control) and then sacrificed at 72 h. (A) *Cd36 and Mrs1/Cd204* mRNA levels in hepatic tissue were assessed using RT-qPCR. (B) Representative western blot and (C) quantification of protein levels of CD36; MRS-1/CD204 in hepatic tissue lysates. (D) *Pcsk9* mRNA levels in hepatic tissues were assessed using RT-qPCR. (E) LDLR protein expression in paraffin-embedded liver sections was evaluated using immunohistochemistry. Figures show a representative mouse from each group. Scale bar, 100 μm. (F) Representative western blot and quantification of protein levels of LDLR and PCSK9 in hepatic tissue lysates. Mean ± SEM of five to eight mice per group, $^{*}p < 0.05$; $^{**}p < 0.01$ versus control. In other sets of experiments, HepG2 cells were stimulated with heme (5 μM) for 24 h. (G) *CD36* mRNA levels in HepG2 cells were assessed using RT-qPCR. (H) Protein levels of CD36 and MRS-1/CD204 assessed using western blotting. (I) Protein levels of LDLR and PCSK9 assessed using western blotting. GAPDH levels were used as loading control. MRS1 and LDLR blots in (B) and (F) have the same loading control (GAPDH). Figure shows a representative western blot and data quantification. Mean ± SEM of three to six experiments, $^{**}p < 0.01$; $^{***}p < 0.001$ versus control.

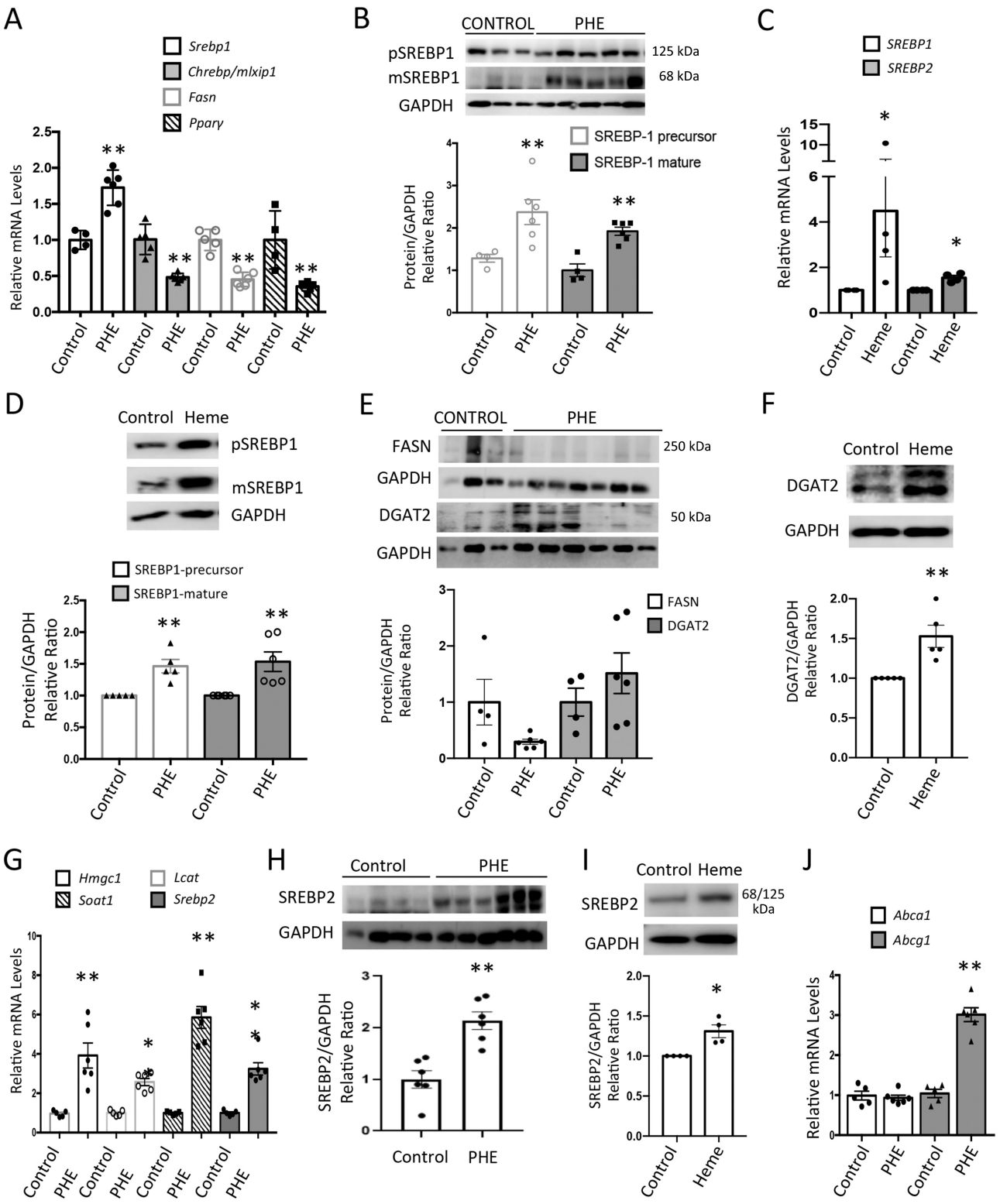

Figure 4. Intravascular hemolysis increases hepatic DNL factors, cholesterol biosynthesis, and the transport/efflux of active cholesterol in mice and HepG2 cells. Mice were injected with PHE (150 mg/kg) or saline (control) and then sacrificed after 72 h. (A) *Srebp1*; *Chrebp/mLxip1; Fasn* and *Pparg* mRNA levels were assessed in hepatic tissue using RT-qPCR. (B) Representative western blot and quantification of precursor (p) and mature (m) SREBP1 protein levels in hepatic tissue lysates. (C) *SREBP1* and *SREBP2* mRNA levels in HepG2 cells stimulated with heme (5 μM) for 24 h were assessed using RT-qPCR. (D) Protein levels of precursor (p) and mature (m) SREBP1 assessed using western blotting. (E) Protein levels of FASN and DGAT2 using western blotting. (F) Protein levels of DGAT2 were assessed using western blotting in HepG2 cells stimulated with heme (5 μM) for 24 h. (G) Hepatic levels of cholesterol biosynthesis mRNAs *Hmgc1*, *Lcat*, *Soat1*, and *Srebp2* were assessed using RT-qPCR. (H) Protein levels of SREBP2 assessed using western blotting in PHE-injected mice and controls. (I) Protein levels of SREBP2 in HepG2 cells stimulated with heme (5 μM) for 24 h were assessed by western blotting. (J) *Abca1* and *Abgc1* mRNA levels in hepatic tissue were assessed using RT-qPCR. GAPDH levels were used as loading control. Figure shows a representative western blot and the quantification of the data. Mean ± SEM of five to eight mice per group, $^{*}p < 0.05$; $^{**}p < 0.01$ versus control, or as the mean ± SEM of three to six experiments, $^{*}p < 0.05$; $^{**}p < 0.01$ versus control.

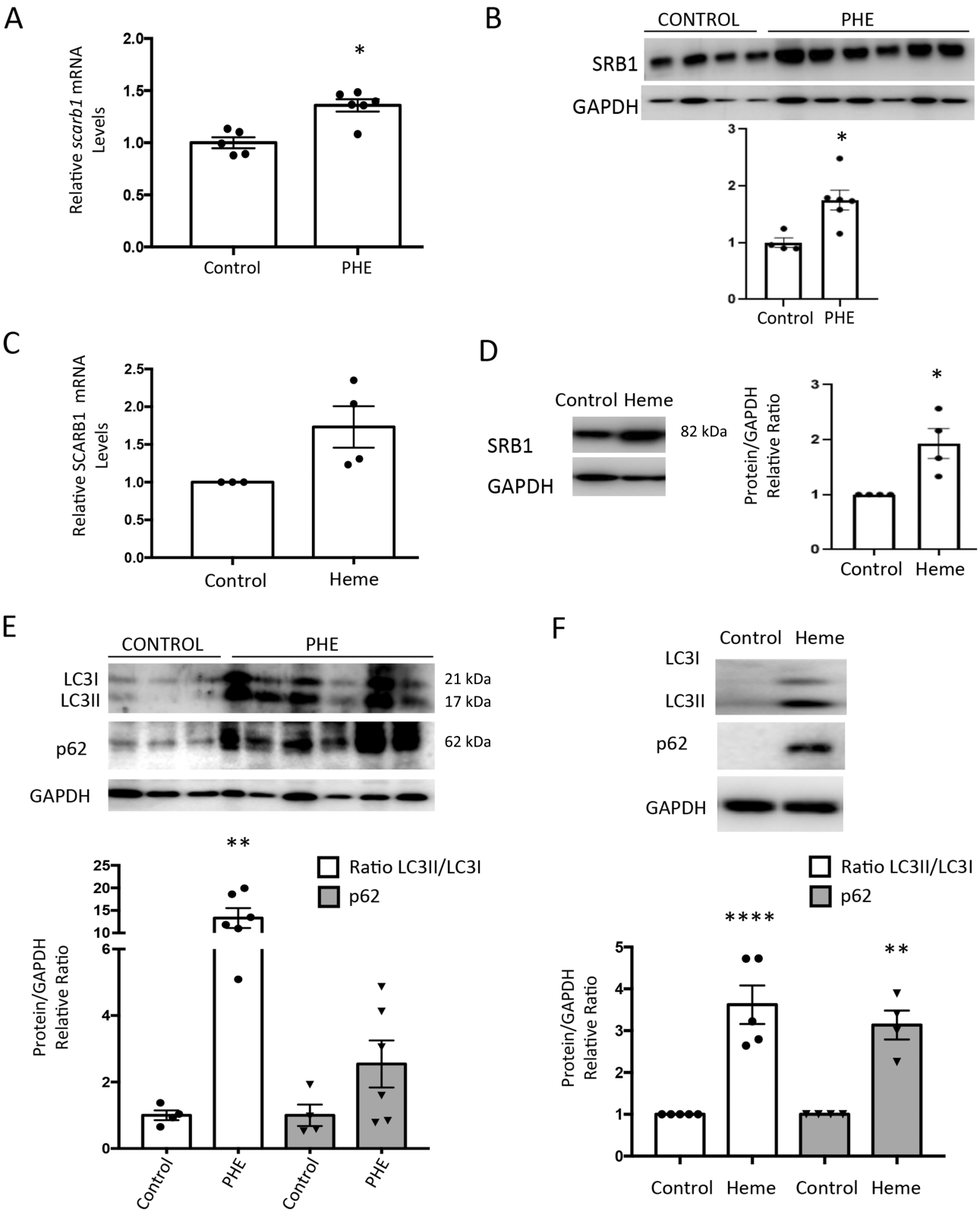

Figure 5. Intravascular hemolysis increases reverse cholesterol transport and blocks autophagosome maturation in mice liver and HepG2 cells. Mice were injected with PHE (150 mg/kg) or saline (control) and sacrificed after 72 h. (A) *Scarb1* mRNA levels in hepatic tissue were assessed using RT-qPCR. (B) Protein levels of SRB1 assessed using western blotting. (C) HepG2 cells were stimulated with heme (5 μM) for 24 h. *Scarb1* mRNA levels were assessed using RT-qPCR. (D) Protein levels of SRB1 assessed using western blotting. (E) Representative western blot and quantification of protein levels of LC3II/LC3I ratio and p62/SQSTM1 in hepatic tissue lysates. Mean ± SEM of five to eight mice per group, $^{**}p < 0.01$ versus control. (F) HepG2 cells were stimulated with heme (5 μM) for 24 h to determine LC3II/LC3I ratio and p62/SQSTM1 protein levels using western blotting. GAPDH levels were used as loading control. Figure shows a representative western blot and the quantification of the data. Mean ± SEM of three to six experiments, $^{**}p < 0.01$; $^{****}p < 0.0001$ versus control.

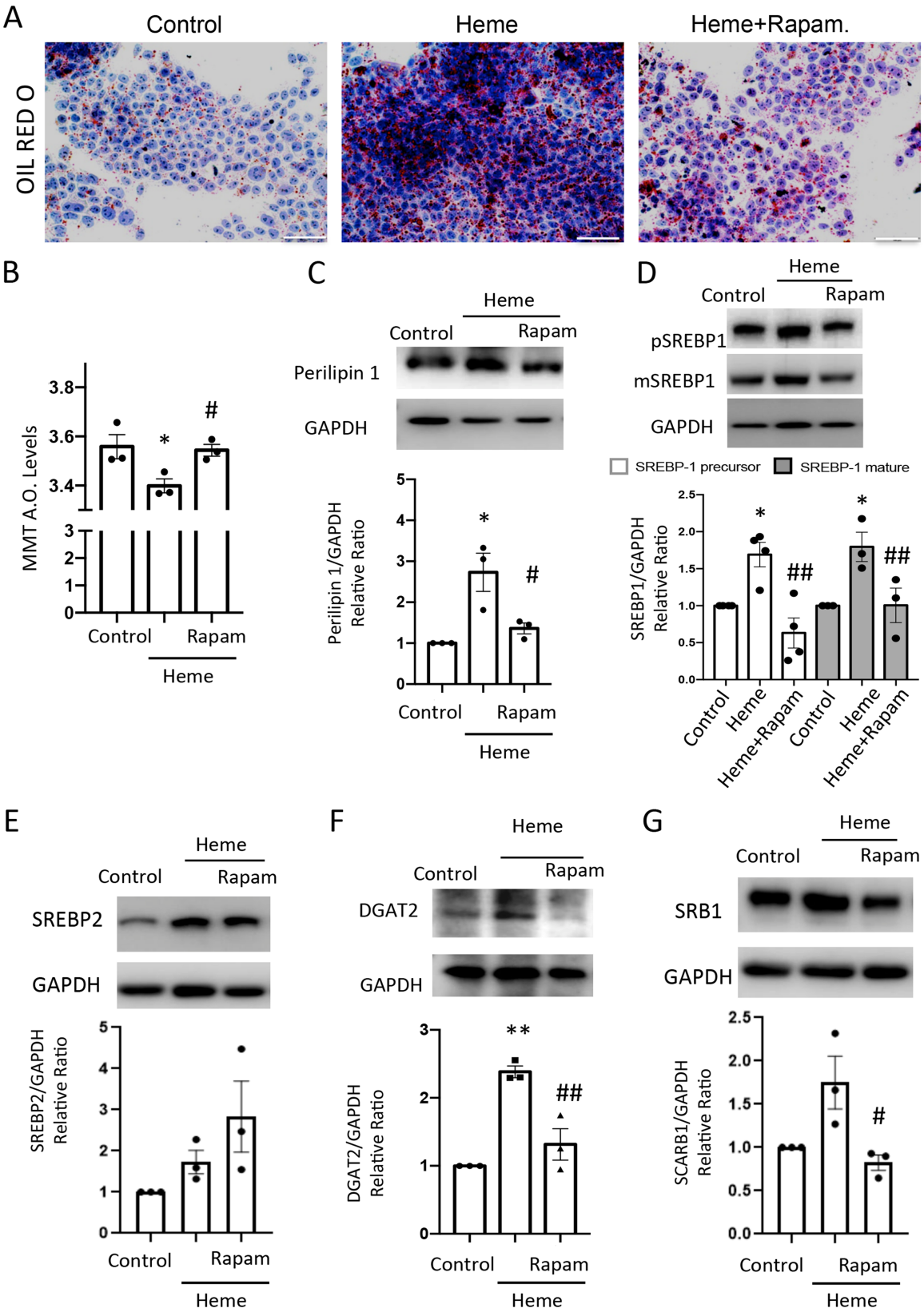

Figure 6. The induction of lipophagy by rapamycin diminishes heme-mediated toxicity, lipid deposition, DNL markers, cholesterol biosynthesis, and reverse cholesterol transport in cultured hepatocytes. HepG2 cells were pretreated with rapamycin (1 μM) for 1 h and then exposed to heme (5 μM) for 24 h. (A) Lipid deposition was evaluated in HepG2 cells by Oil Red O staining. Figures show a representative image from each experimental condition. Scale bar, 100 μm. (B) Viability assay of HepG2 cells assessed by MTT staining. (C) Protein levels of Perilipin 1 assessed using western blotting. GAPDH levels were used as loading controls. Figure shows a representative western blot and quantification of data. (D) Representative western blot and quantification of protein levels of precursor (p) and mature (m) SREBP1 in HepG2 cell lysates. Protein levels of (E) SREBP2, (F) DGAT2, and (G) SRB1 assessed using western blotting. Mean ± SEM of three to six experiments, $^{*}p < 0.05$; $^{**}p < 0.01$ versus control. $\#p < 0.05$; $\#\#p < 0.01$ versus heme.

hemolysis fed with ^{13}C-acetate showed a trend nonsignificant enrichment of labeled cholesterol compared to healthy mice treated with this tracer (no variation was observed in control/hemolysis animals fed with unlabeled acetate).

Intravascular hemolysis increases cholesterol efflux and reverse transport in the liver

We also analyzed the gene expression of ATP-binding cassette subfamily A member 1 (*Abca1*) and subfamily G member 1 (*Abcg1*). In livers from mice subjected to intravascular hemolysis, we observed a clear upregulation of *Abcg1*, while no significant changes were observed in *Abca1* (Figure 4J). In addition to cholesterol reverse transport, we also analyzed the gene expression levels of the receptor scavenger SRB1. We observed increased mRNA and protein levels of the *Scarb1/SRB1* in PHE-injected mice (Figure 5A,B) and heme-stimulated hepatocytes (Figure 5C,D).

Intravascular hemolysis impairs hepatic lipophagy by blocking autophagosome maturation *in vivo* and in cultured hepatocytes

We analyzed the role of autophagy in the deregulation of lipid metabolism associated with intravascular hemolysis. To this end, we studied the protein levels of some key regulators of the autophagy-signaling pathway, such as LC3I, LC3II, and p62/SQSTM1. We found an increased LC3II/LC3I ratio in PHE-injected mice, indicating an increase of autophagosome content (Figure 5E). On the other hand, p62/SQSTM1 protein levels were also increased in response to intravascular hemolysis, indicating a blockade of autophagosome-lysosome fusion pathway and the consequent accumulation of autophagy substrates in the liver (Figure 5E). Similar results were observed in heme-stimulated hepatocytes (Figure 5F).

Induction of lipophagy by rapamycin diminished lipid deposition and reverse cholesterol transport in cultured hepatocytes

Finally, we analyzed whether the induction of autophagy by rapamycin ameliorated heme-mediated harmful effects. In HepG2 cells, rapamycin reduced heme-mediated microvesicular lipid content (Figure 6A), toxicity (Figure 6B), and Perilipin 1 content (Figure 6C). We next analyzed the effects of rapamycin on metabolic pathways altered in response to heme. Interestingly, rapamycin reduced heme-mediated upregulation of the precursor and mature form of SREBP1 (Figure 6D) and DGAT2 (Figure 6F), whereas no differences were reported in SREBP2 protein expression (Figure 6E). Finally, rapamycin also downregulated reverse cholesterol transport induced by heme (Figure 6G).

Discussion

In this article we have demonstrated, for the first time, the dysregulation of lipid metabolism and development of liver steatosis in a preclinical model of intravascular hemolysis. In the liver, overload of Hb and its heme derivates promotes hepatic accumulation of lipids, mainly derived from increased lipid uptake and cholesterol synthesis but not from DNL. These pathogenic mechanisms may be associated with the dysregulation of autophagy and may be involved in the progression of hepatic damage in patients with severe hemolytic crisis.

The liver is involved in the scavenging of senescent red blood cells, cell-free Hb and heme, and iron recycling [38]. However, exacerbated release of heme derivates during massive intravascular hemolysis results in the accumulation of these toxic molecules in the liver, promoting deleterious side effects [3–5,7]. Clinical studies reported liver injury in 10–40% of patients with SCD [8]. Hepatic damage was also observed in animals affected by SCD [39], malaria [40], or other hemolytic entities [9,11,12]. In these pathological settings, hepatic injury was characterized by the presence of necrotic areas, lipid peroxidation, inflammation, and elevated serum bilirubin levels [41–45]. In our experimental model, intravascular hemolysis triggered liver injury, as demonstrated by a marked increase of serum transaminases and histological alterations, including hepatocellular ballooning, microvesicular steatosis, and inflammatory clusters, as well as exacerbated expression of inflammatory mediators and markers of oxidative stress. Exposure of cultured hepatocytes to heme increased oxidative stress and promoted inflammatory cytokine release, confirming the deleterious effect of heme derivates in the liver.

The liver also plays a key role in the regulation of lipid metabolism. However, the effects of hemolysis on lipid metabolism are not fully understood. Some studies have described the presence of hypocholesterolemia in patients with SCD [46–48], whereas another has reported opposite results [49]. Our results showed increased serum concentrations of total cholesterol, LDL-c, HDL-c, and TGs, as well as increased deposition of lipid droplets in the liver of mice with intravascular hemolysis. Similar results were observed in heme-stimulated hepatocytes, where we also reported increased Perilipin 1 expression, one of the proteins responsible of lipid droplet coating. Induction of hemolysis also increased fatty acid levels in liver, mainly oleic, palmitoleic, and palmitic acid. These molecules have been found elevated in livers from NAFLD patients, being related to hepatic lipotoxicity [50–52]. In fact, upregulation of lipogenesis has been associated with NAFLD development [36,53–57]. There is little information about the presence of liver steatosis in patients with intravascular hemolysis. A few studies have reported fatty changes in the liver from patients with SCD [58,59] or malaria [60–63]. Hepatic infiltration of fatty acids was also reported in rare cases of acute hemolytic syndromes [64–66]. Thus, this limited amount of

evidence suggests that it is necessary to validate our results before confirming their translational relevance.

Hepatic damage could be associated with an imbalance between the synthesis and catabolism of lipids, triggering the accumulation of toxic lipidic species that may promote inflammation, oxidative stress, and cell death [67]. Several lipid-associated metabolic changes have been reported in NAFLD, including increased fatty acid uptake, DNL, and TG synthesis [68]. We explored whether these metabolic pathways were disturbed in response to hemolysis, to gain insight on the increased lipid content observed in the liver. The transcriptional regulation of DNL is mainly directed by two transcription factors: SREBP1 and ChREBP/mLxip1 [69–71]. We observed a significant increase at the gene and protein levels of SREBP1 and a reduction in gene expression of *ChREBP/mLxip1* in mice subjected to intravascular hemolysis. These changes may induce dysregulation of key enzymes involved in the synthesis of cholesterol and TGs, such as HMGC1, LCAT, and the factor responsible for controlling cholesterol biosynthesis, SREBP2, as reported in our article. We also observed that hemolysis elicited liver expression of CD36 and MSR1, receptors involved in lipid uptake of long-chain fatty acids [36]. Similar results were obtained in cultured hepatocytes stimulated with heme, suggesting increased lipid transport in response to heme. Such marked uptake was coupled to increased TG synthesis, attested by the increase in DGAT2 *in vivo* and *in vitro*. We finally explored whether the increased fatty acid deposition in liver from mice with hemolysis was driven by hepatic DNL. Our results seem to reject such a hypothesis, given the significant reduction of FASN (a multifunctional enzyme that specifically catalyzes DNL), and the lack of differences between control and treated mice regarding transformation of labeled dietary acetate into hepatic fatty acids.

The transport and efflux of cholesterol play an important role in hepatic lipid homeostasis [72]. ABCA1 and ABCG1 are involved in cholesterol efflux and intracellular cholesterol homeostasis using ATP to transport fatty acids from the inner part of the plasma membrane to extracellular lipophilic acceptors, such as apolipoproteins or HDL. In the hemolysis group, we observed an upregulation of *Abcg1* gene expression, but not for *Abca1*. Studies in mice fed a high-cholesterol diet demonstrated upregulation of *Abcg1* expression in parenchymal liver cells, whereas the gene blockade of this molecule induced hepatic lipid accumulation [73–75]. The SR-BI is a scavenger receptor associated with the selective uptake or influx of HDL-derived cholesteryl esters and other lipids from HDLs and LDLs to cells [76,77]. Interestingly, hemolysis increased gene and protein expression of SR-B1, suggesting dysregulation of reverse cholesterol transport. PCSK9 is a circulating serine protease that effectively binds to LDLR and leads to its intracellular degradation in the liver [78]. Therefore, increased PCSK9 levels may impair liver LDL uptake, resulting in increased LDL cholesterol plasma concentration [37]. We also demonstrated diminished hepatic LDL uptake in response to hemolysis, as demonstrated by reduced gene and protein levels of LDLR and increased hepatic expression of PCSK9, a protease that blocks intracellular degradation of LDLR [37]. Since decreased LDL uptake contributes to hypercholesterolemia [79,80], these results may explain the elevated serum LDL-c levels observed after induction of hemolysis.

Another key finding of our study is the alteration of autophagy as a mechanism associated with liver toxicity in response to intravascular hemolysis. Excessive lipid accumulation in the liver induces toxicity and NAFLD [81–84]. Autophagy restrains the deleterious effects of lipid species by promoting their degradation in lysosomes (lipophagy) [30]. LC3-II levels, one of the components of the autophagosomal membranes, reflect the balance in the autophagosome turnover, but cannot represent the autophagy flux [85]. In contrast, p62/SQSTM1 is a substrate in the autophagic process and a key protein in autophagic flux [86]. The accumulation of p62/SQTSM1 in hepatic cells of NAFLD patients indicated autophagy flux blockage [87]. *In vitro* studies in endothelial cells stimulated with heme demonstrated that the blockade of autophagy increased cell death and promoted damage *via* induction of lipid peroxidation [88]. Accordingly, we demonstrated that heme accumulation hastened the autophagy process in response to liver damage, modulating LC3II/LC3I ratio and p62/SQSTM1 both *in vivo* and *in vitro*. These observations suggest that hemolysis increased autophagosome formation but disrupted autophagic flux by the accumulation of p62/SQSTM1. The beneficial effects of activation of autophagy against liver damage are well known [31,89]. A crosstalk between the autophagic process and lipid homeostasis was described to provide energy and essential substrates for liver functions. Breaking down lipid droplets compensates for the lack of energy in the liver by lipophagy [90,91]. The blockade of autophagy *in vivo* and *in vitro* increased triacylglycerols and LDL levels [91]. In addition, a study in an animal model of nonalcoholic steatohepatitis showed that the modulation of the mTORC1 signaling pathway protected from hepatic steatosis through the control of lipid export and DNL [92]. The use of rapamycin (mTOR inhibitor) in mice with NAFLD also ameliorated hepatic steatosis and liver injury by diminishing DNL and promoting PPARα-mediated fatty acid oxidation [93]. In accordance with this, our study demonstrated that rapamycin reduced heme-mediated hepatotoxicity and decreased the accumulation of microvesicular lipid droplets and Perilipin 1 protein levels in HepG2 cells. In addition, the treatment of HepG2 cells with rapamycin reduced the protein levels of SREBP1 and one of the enzymes that regulate the synthesis of TGs, DGAT2. We also observed a reduction of heme-mediated SR-B1 upregulation in cells pretreated with rapamycin, suggesting a modulation of reverse cholesterol transport.

In conclusion, this study demonstrated that the hepatotoxic effect of heme accumulation, as a consequence of intravascular hemolysis, triggered NAFLD.

Thus, intravascular hemolysis deregulated lipid metabolism, producing increased hepatic TG accumulation, cholesterol biosynthesis, LDLR/PCSK9 modulation, and regulation of reverse cholesterol transport. In studies in hepatocytes, we identified the impairment of lipophagy as a consequence of heme accumulation, demonstrating that autophagy induction by rapamycin could be a potential therapeutic option to reduce the deleterious effects of intravascular hemolysis by modulating lipid homeostasis (Figure S5). However, additional studies in animal models of intravascular hemolysis are needed to corroborate these potential beneficial effects of autophagy inducers. Despite this limitation, the findings revealed by our study may have high translational value as a novel NAFLD-promoting mechanism in patients suffering from severe hemolysis episodes.

Acknowledgements

This research was funded by Instituto de Salud Carlos III (ISCIII, FIS-FEDER PI17/00130, PI20/00375, PI20/00487, PI20/00140, RICORS2040, RD21/0005/0002 and DTS19/00093) (co-funded by European Regional Development Fund/European Social Fund 'A way to make Europe'/'Investing in your future'), Spanish Biomedical Research Centre in Diabetes and Associated Metabolic Disorders (CIBERDEM) and in Cardiovascular Diseases (CIBERCV), Spanish Societies of Cardiology (SEC), Nephrology (SEN), and Atherosclerosis (SEA). Consejería de Salud y Familias-FEDER, Junta de Andalucía (PIGE-0052-2020). The Sara Borrell training program of the ISCIII and Juan de la Cierva training program of the MINECO supported the salary of SR-M at different time points (CD19/00021; IJC2018-035187-I). The Spanish Ministry of Science and Innovation supported the salary of JAM (RYC-2017-22369) and JLM-P (FJC2019-042028-I) (co-funded by European Regional Development Fund/European Social Fund 'A way to make Europe'/'Investing in your future'). Córdoba University supported the salary of CGC. Funding for open access charge: Universidad de Córdoba/CBUA.

Author contributions statement

The authors contributed in the following way: SR-M contributed to the design of the experiments, to the acquisition, analysis and interpretation of all data, and drafted the manuscript. JLM-P, CG-C, IL, AS-V, SM-F and LO-R contributed to the acquisition of data and participated in the development of mouse models and analysis of the data. MR-O and JE contributed to the critical review of the manuscript and obtaining financial support for the work. JAM contributed to the design of the experiments, the interpretation of the data, drafting the manuscript, and obtaining financial support for the work. All authors read and agreed to the published version of the manuscript.

Data availability statement

No multiomics data were obtained in this article. Results used in this publication will be shared upon reasonable request addressed to the corresponding author.

References

1. Moreno JA, Martín-Cleary C, Gutiérrez E, *et al*. AKI associated with macroscopic glomerular hematuria: clinical and pathophysiologic consequences. *Clin J Am Soc Nephrol* 2012; **7:** 175–184.
2. Kato GJ, Taylor JG VI. Pleiotropic effects of intravascular haemolysis on vascular homeostasis. *Br J Haematol* 2010; **148:** 690–701.
3. Belcher JD, Beckman JD, Balla G, *et al*. Heme degradation and vascular injury. *Antioxid Redox Signal* 2010; **12:** 233–248.
4. Woollard KJ, Sturgeon S, Chin-Dusting JPF, *et al*. Erythrocyte hemolysis and hemoglobin oxidation promote ferric chloride-induced vascular injury. *J Biol Chem* 2009; **284:** 13110–13118.
5. Qian Q, Nath KA, Wu Y, *et al*. Hemolysis and acute kidney failure. *Am J Kidney Dis* 2010; **56:** 780–784.
6. Yang F, Haile DJ, Berger FG, *et al*. Haptoglobin reduces lung injury associated with exposure to blood. *Am J Physiol Lung Cell Mol Physiol* 2003; **284:** L402-9.
7. Tolosano E, Fagoonee S, Hirsch E, *et al*. Enhanced splenomegaly and severe liver inflammation in haptoglobin/hemopexin double-null mice after acute hemolysis. *Blood* 2002; **100:** 4201–4208.
8. Shah R, Taborda C, Chawla S. Acute and chronic hepatobiliary manifestations of sickle cell disease: a review. *World J Gastrointest Pathophysiol* 2017; **8:** 108.
9. Teixeira RS, Arriaga MB, Terse-Ramos R, *et al*. Higher values of triglycerides:HDL-cholesterol ratio hallmark disease severity in children and adolescents with sickle cell anemia. *Braz J Med Biol Res* 2019; **52:** e8833.
10. Merle NS, Paule R, Leon J, *et al*. P-selectin drives complement attack on endothelium during intravascular hemolysis in TLR-4/heme-dependent manner. *Proc Natl Acad Sci U S A* 2019; **116:** 6280–6285.
11. Panda H, Keleku-Lukwete N, Kuga A, *et al*. Dietary supplementation with sulforaphane attenuates liver damage and heme overload in a sickle cell disease murine model. *Exp Hematol* 2019; **77:** 51–60.e1.
12. Hanson MS, Xu H, Flewelen TC, *et al*. A novel hemoglobin-binding peptide reduces cell-free hemoglobin in murine hemolytic anemia. *Am J Physiol Heart Circ Physiol* 2013; **304:** H328-36.
13. Abdel-Maboud M, Menshawy A, Menshawy E, *et al*. The efficacy of vitamin E in reducing non-alcoholic fatty liver disease: a systematic review, meta-analysis, and meta-regression. *Therap Adv Gastroenterol* 2020; **13:** 1756284820974917.
14. Cariou B, Byrne CD, Loomba R, *et al*. Nonalcoholic fatty liver disease as a metabolic disease in humans: a literature review. *Diabetes Obes Metab* 2021; **23:** 1069–1083.
15. Haas JT, Francque S, Staels B. Pathophysiology and mechanisms of nonalcoholic fatty liver disease. *Annu Rev Physiol* 2016; **78:** 181–205.
16. Opazo-Ríos L, Soto-Catalán M, Lázaro I, *et al*. Meta-inflammation and de novo lipogenesis markers are involved in metabolic associated fatty liver disease progression in BTBR Ob/Ob mice. *Int J Mol Sci* 2022; **23:** 3965.
17. Ipsen DH, Lykkesfeldt J, Tveden-Nyborg P. Molecular mechanisms of hepatic lipid accumulation in non-alcoholic fatty liver disease. *Cell Mol Life Sci* 2018; **75:** 3313–3327.
18. Yang S, Chen XY, Xu XP. The relationship between lipoprotein-associated phospholipase A(2), cholesteryl ester transfer protein and lipid profile and risk of atherosclerosis in women with iron deficiency anaemia. *Clin Lab* 2015; **61:** 1463–1469.

19. Shirvani M, Sadeghi MV, Hosseini SR, *et al*. Does serum lipid profile differ in anemia and non-anemic older subjects? *Caspian J Intern Med* 2017; **8:** 305–310.
20. Kelesidis T, Currier JS. Dyslipidemia and cardiovascular risk in human immunodeficiency virus infection. *Endocrinol Metab Clin North Am* 2014; **43:** 665–684.
21. Katsiki N, Mikhailidis DP, Mantzoros CS. Non-alcoholic fatty liver disease and dyslipidemia: an update. *Metabolism* 2016; **65:** 1109–1123.
22. Diamanti-Kandarakis E, Papavassiliou AG, Kandarakis SA, *et al*. Pathophysiology and types of dyslipidemia in PCOS. *Trends Endocrinol Metab* 2007; **18:** 280–285.
23. Kaplan BS, Gale D, Ipp T. Hyperlipidemia in the hemolytic-uremic syndrome. *Pediatrics* 1971; **47:** 776–779.
24. Choudhry F, Kathawa J, Kerton K, *et al*. Zieve's syndrome presenting with severe hypertriglyceridemia. *ACG Case Rep J* 2019; **6:** e00133.
25. Hartman C, Tamary H, Tamir A, *et al*. Hypocholesterolemia in children and adolescents with beta-thalassemia intermedia. *J Pediatr* 2002; **141:** 543–547.
26. Glick D, Barth S, Macleod KF. Autophagy: cellular and molecular mechanisms. *J Pathol* 2010; **221:** 3–12.
27. Levy JMM, Towers CG, Thorburn A. Targeting autophagy in cancer. *Nat Rev Cancer* 2017; **17:** 528–542.
28. Kim KH, Lee MS. Autophagy–a key player in cellular and body metabolism. *Nat Rev Endocrinol* 2014; **10:** 322–337.
29. Ueno T, Komatsu M. Autophagy in the liver: functions in health and disease. *Nat Rev Gastroenterol Hepatol* 2017; **14:** 170–184.
30. Martinez-Lopez N, Singh R. Autophagy and lipid droplets in the liver. *Annu Rev Nutr* 2015; **35:** 215–237.
31. Allaire M, Rautou PE, Codogno P, *et al*. Autophagy in liver diseases: time for translation? *J Hepatol* 2019; **70:** 985–998.
32. Williams JA, Ding WX. Role of autophagy in alcohol and drug-induced liver injury. *Food Chem Toxicol* 2020; **136:** 111075.
33. Rubio-Navarro A, Vázquez-Carballo C, Guerrero-Hue M, *et al*. Nrf2 plays a protective role against intravascular hemolysis-mediated acute kidney injury. *Front Pharmacol* 2019; **10:** 740.
34. Agren JJ, Julkunen A, Penttilä I. Rapid separation of serum lipids for fatty acid analysis by a single aminopropyl column. *J Lipid Res* 1992; **33:** 1871–1876.
35. Shimomura I, Shimano H, Korn BS, *et al*. Nuclear sterol regulatory element-binding proteins activate genes responsible for the entire program of unsaturated fatty acid biosynthesis in transgenic mouse liver. *J Biol Chem* 1998; **273:** 35299–35306.
36. Koo SH. Nonalcoholic fatty liver disease: molecular mechanisms for the hepatic steatosis. *Clin Mol Hepatol* 2013; **19:** 210–215.
37. Sahng WP, Moon YA, Horton JD. Post-transcriptional regulation of low density lipoprotein receptor protein by proprotein convertase subtilisin/kexin type 9a in mouse liver. *J Biol Chem* 2004; **279:** 50630–50638.
38. Corrons JLV, Casafont LB, Frasnedo EF. Concise review: how do red blood cells born, live, and die? *Ann Hematol* 2021; **100:** 2425–2433.
39. Wu LC, Sun CW, Ryan TM, *et al*. Correction of sickle cell disease by homologous recombination in embryonic stem cells. *Blood* 2006; **108:** 1183–1188.
40. Dey S, Bindu S, Goyal M, *et al*. Impact of intravascular hemolysis in malaria on liver dysfunction: involvement of hepatic free heme overload, NF-κB activation, and neutrophil infiltration. *J Biol Chem* 2012; **287:** 26630–26646.
41. McMillan DC, Jensen CB, Jollow DJ. Role of lipid peroxidation in dapsone-induced hemolytic anemia. *J Pharmacol Exp Ther* 1998; **287:** 868–876.
42. Jain SK, Subrahmanyam D. On the mechanism of phenylhydrazine-induced hemolytic anemia. *Biochem Biophys Res Commun* 1978; **82:** 1320–1324.
43. Pejnovic N, Jeftic I, Jovicic N, *et al*. Galectin-3 and IL-33/ST2 axis roles and interplay in diet-induced steatohepatitis. *World J Gastroenterol* 2016; **22:** 9706–9717.
44. Gao Y, Liu Y, Yang M, *et al*. IL-33 treatment attenuated diet-induced hepatic steatosis but aggravated hepatic fibrosis. *Oncotarget* 2016; **7:** 33649–33661.
45. Yazdani HO, Chen HW, Tohme S, *et al*. IL-33 exacerbates liver sterile inflammation by amplifying neutrophil extracellular trap formation. *J Hepatol* 2017; **68:** 130–139.
46. Yalcinkaya A, Unal S, Oztas Y. Altered HDL particle in sickle cell disease: decreased cholesterol content is associated with hemolysis, whereas decreased apolipoprotein A1 is linked to inflammation. *Lipids Health Dis* 2019; **18:** 225.
47. Rahimi Z, Merat A, Haghshenass M, *et al*. Plasma lipids in Iranians with sickle cell disease: hypocholesterolemia in sickle cell anemia and increase of HDL-cholesterol in sickle cell trait. *Clin Chim Acta* 2006; **365:** 217–220.
48. Vendrame F, Olops L, Saad STO, *et al*. Hypocholesterolemia and dysregulated production of angiopoietin-like proteins in sickle cell anemia patients. *Cytokine* 2019; **120:** 88–91.
49. Djoumessi S, Zekeng L, Lando G, *et al*. Serum lipids and atherogenic risk in sickle-cell trait carriers. *Ann Biol Clin (Paris)* 1994; **52:** 663–665.
50. Puri P, Baillie RA, Wiest MM, *et al*. A lipidomic analysis of nonalcoholic fatty liver disease. *Hepatology* 2007; **46:** 1081–1090.
51. Moravcová A, Červinková Z, Kučera O, *et al*. The effect of oleic and palmitic acid on induction of steatosis and cytotoxicity on rat hepatocytes in primary culture. *Physiol Res* 2015; **64:** S627–S636.
52. Pardo V, González-Rodríguez Á, Muntané J, *et al*. Role of hepatocyte S6K1 in palmitic acid-induced endoplasmic reticulum stress, lipotoxicity, insulin resistance and in oleic acid-induced protection. *Food Chem Toxicol* 2015; **80:** 298–309.
53. Diraison F, Moulin PH, Beylot M. Contribution of hepatic de novo lipogenesis and reesterification of plasma non esterified fatty acids to plasma triglyceride synthesis during non-alcoholic fatty liver disease. *Diabetes Metab* 2003; **29:** 478–485.
54. Lambert JE, Ramos-Roman MA, Browning JD, *et al*. Increased de novo lipogenesis is a distinct characteristic of individuals with nonalcoholic fatty liver disease. *Gastroenterology* 2014; **146:** 726–735.
55. Tamura S, Shimomura I. Contribution of adipose tissue and de novo lipogenesis to nonalcoholic fatty liver disease. *J Clin Invest* 2005; **115:** 1139–1142.
56. Donnelly KL, Smith CI, Schwarzenberg SJ, *et al*. Sources of fatty acids stored in liver and secreted via lipoproteins in patients with nonalcoholic fatty liver disease. *J Clin Invest* 2005; **115:** 1343–1351.
57. Kohjima M, Enjoji M, Higuchi N, *et al*. Re-evaluation of fatty acid metabolism-related gene expression in nonalcoholic fatty liver disease. *Int J Mol Med* 2007; **20:** 351–358.
58. Aken'ova YA, Olasode J, Ogunbiyi JO, *et al*. Hepatobiliary changes in Nigerians with sickle cell anaemia. *Ann Trop Med Parasitol* 1993; **87:** 603–606.
59. Hernández C, Ruiz ME, Gaecía Tamayo J. Sickle-cell anemia. The liver lesions. A clinical, morphological and ultrastructural study of 21 cases. *G E N* 1992; **46:** 183–190 [Article in Spanish].
60. Chawla LS, Sidhu G, Sabharwal BD, *et al*. Jaundice in *Plasmodium falciparum*. *J Assoc Physicians India* 1989; **37:** 390–391.
61. Kochar DK, Singh P, Agarwal P, *et al*. Malarial hepatitis. *J Assoc Physicians India* 2003; **51:** 1069–1072.
62. Das SN, Mohapatra B, Mohanty R, *et al*. Malarial hepatitis as a component of multiorgan failure–a bad prognostic sign. *J Indian Med Assoc* 2007; **105:** 247–250.
63. Rupani AB, Amarapurkar AD. Hepatic changes in fatal malaria: an emerging problem. *Ann Trop Med Parasitol* 2009; **103:** 119–127.

64. Ang SX, Chen CP, Sun FJ, *et al*. Comparison of maternal and neonatal outcomes between acute fatty liver of pregnancy and hemolysis, elevated liver enzymes and low platelets syndrome: a retrospective cohort study. *BMC Pregnancy Childbirth* 2021; **21:** 293.
65. Rametta R, Fracanzani AL, Fargion S, *et al*. Dysmetabolic hyperferritinemia and dysmetabolic iron overload syndrome (DIOS): two related conditions or different entities? *Curr Pharm Des* 2020; **26:** 1025–1035.
66. Ibdah JA. Acute fatty liver of pregnancy: an update on pathogenesis and clinical implications. *World J Gastroenterol* 2006; **12:** 7397–7404.
67. Ekstedt M, Hagström H, Nasr P, *et al*. Fibrosis stage is the strongest predictor for disease-specific mortality in NAFLD after up to 33 years of follow-up. *Hepatology* 2015; **61:** 1547–1554.
68. Geng Y, Faber KN, de Meijer VE, *et al*. How does hepatic lipid accumulation lead to lipotoxicity in non-alcoholic fatty liver disease? *Hepatol Int* 2021; **15:** 21–35.
69. Sanders FWB, Griffin JL. De novo lipogenesis in the liver in health and disease: more than just a shunting yard for glucose. *Biol Rev Camb Philos Soc* 2016; **91:** 452–468.
70. Eberlé D, Hegarty B, Bossard P, *et al*. SREBP transcription factors: master regulators of lipid homeostasis. *Biochimie* 2004; **86:** 839–848.
71. Yamashita H, Takenoshita M, Sakurai M, *et al*. A glucose-responsive transcription factor that regulates carbohydrate metabolism in the liver. *Proc Natl Acad Sci U S A* 2001; **98:** 9116–9121.
72. Hardy LM, Frisdal E, Le Goff W. Critical role of the human ATP-binding cassette G1 transporter in cardiometabolic diseases. *Int J Mol Sci* 2017; **18:** 1892.
73. Hoekstra M, Kruijt JK, Van Eck M, *et al*. Specific gene expression of ATP-binding cassette transporters and nuclear hormone receptors in rat liver parenchymal, endothelial, and Kupffer cells. *J Biol Chem* 2003; **278:** 25448–25453.
74. Kennedy MA, Barrera GC, Nakamura K, *et al*. ABCG1 has a critical role in mediating cholesterol efflux to HDL and preventing cellular lipid accumulation. *Cell Metab* 2005; **1:** 121–131.
75. Wiersma H, Nijstad N, de Boer JF, *et al*. Lack of Abcg1 results in decreased plasma HDL cholesterol levels and increased biliary cholesterol secretion in mice fed a high cholesterol diet. *Atherosclerosis* 2009; **206:** 141–147.
76. Greene DJ, Skeggs JW, Morton RE. Elevated triglyceride content diminishes the capacity of high density lipoprotein to deliver cholesteryl esters via the scavenger receptor class B type I (SR-BI). *J Biol Chem* 2001; **276:** 4804–4811.
77. Swarnakar S, Temel RE, Connelly MA, *et al*. Scavenger receptor class B, type I, mediates selective uptake of low density lipoprotein cholesteryl ester. *J Biol Chem* 1999; **274:** 29733–29739.
78. Sabatine MS. PCSK9 inhibitors: clinical evidence and implementation. *Nat Rev Cardiol* 2019; **16:** 155–165.
79. Hobbs HH, Brown MS, Goldstein JL. Molecular genetics of the LDL receptor gene in familial hypercholesterolemia. *Hum Mutat* 1992; **1:** 445–466.
80. Norum KR, Berg T, Helgerud P, *et al*. Transport of cholesterol. *Physiol Rev* 1983; **63:** 1343–1419.
81. Svegliati-Baroni G, Pierantonelli I, Torquato P, *et al*. Lipidomic biomarkers and mechanisms of lipotoxicity in non-alcoholic fatty liver disease. *Free Radic Biol Med* 2019; **144:** 293–309.
82. Ioannou GN. The role of cholesterol in the pathogenesis of NASH. *Trends Endocrinol Metab* 2016; **27:** 84–95.
83. Carotti S, Aquilano K, Zalfa F, *et al*. Lipophagy impairment is associated with disease progression in NAFLD. *Front Physiol* 2020; **11:** 850.
84. Schulze RJ, Drižytė K, Casey CA, *et al*. Hepatic lipophagy: new insights into autophagic catabolism of lipid droplets in the liver. *Hepatol Commun* 2017; **1:** 359–369.
85. Mizushima N, Yoshimori T, Levine B. Methods in mammalian autophagy research. *Cell* 2010; **140:** 313–326.
86. Watanabe Y, Tanaka M. p62/SQSTM1 in autophagic clearance of a non-ubiquitylated substrate. *J Cell Sci* 2011; **124:** 2692–2701.
87. Fukushima H, Yamashina S, Arakawa A, *et al*. Formation of p62-positive inclusion body is associated with macrophage polarization in non-alcoholic fatty liver disease. *Hepatol Res* 2018; **48:** 757–767.
88. Higdon AN, Benavides GA, Chacko BK, *et al*. Hemin causes mitochondrial dysfunction in endothelial cells through promoting lipid peroxidation: the protective role of autophagy. *Am J Physiol Heart Circ Physiol* 2012; **302:** H1394-409.
89. Xie Y, Xiao F, Luo L, *et al*. Activation of autophagy protects against ROS-mediated mitochondria-dependent apoptosis in L-02 hepatocytes induced by Cr(VI). *Cell Physiol Biochem* 2014; **33:** 705–716.
90. Filali-Mouncef Y, Hunter C, Roccio F, *et al*. The ménage à trois of autophagy, lipid droplets and liver disease. *Autophagy* 2022; **18:** 50–72.
91. Singh R, Kaushik S, Wang Y, *et al*. Autophagy regulates lipid metabolism. *Nature* 2009; **458:** 1131–1135.
92. Uehara K, Sostre-Colón J, Gavin M, *et al*. Activation of liver mTORC1 protects against NASH via dual regulation of VLDL-TAG secretion and de novo lipogenesis. *Cell Mol Gastroenterol Hepatol* 2022; **13:** 1625–1647.
93. Zhao R, Zhu M, Zhou S, *et al*. Rapamycin-loaded mPEG-PLGA nanoparticles ameliorate hepatic steatosis and liver injury in non-alcoholic fatty liver disease. *Front Chem* 2020; **8:** 407.
94. Burdge GC, Wright P, Jones AE, *et al*. A method for separation of phosphatidylcholine, triacylglycerol, non-esterified fatty acids and cholesterol esters from plasma by solid-phase extraction. *Br J Nutr* 2000; **84:** 781–787.
95. Thurnhofer S, Vetter W. A gas chromatography/electron ionization-mass spectrometry-selected ion monitoring method for determining the fatty acid pattern in food after formation of fatty acid methyl esters. *J Agric Food Chem* 2005; **53:** 8896–8903.

References 94 and 95 are cited only in supplementary material.

SUPPLEMENTARY MATERIAL ONLINE

Supplementary materials and methods

Figure S1. Hemin overload induces hepatic damage and lipid deposition in mice

Figure S2. High carbonyl iron diet induces hepatic damage and lipid deposition in mice

Figure S3. Lipid composition in liver after 72 h of experimental intravascular hemolysis [control (red); hemolysis (green)]

Figure S4. Direct determination of *de novo* biosynthesis of fatty acids and cholesterol by GC–MS

Figure S5. Summary scheme indicating effect of intravascular hemolysis in hepatic tissue and beneficial effect of autophagy inductor rapamycin